Published for SISSA by Springer

Received: March 17, 2021
Revised: June 2, 2021
Accepted: June 15, 2021
Published: July 6, 2021

JHEP07(2021)023

NNLO QCD study of polarised W^+W^- production at the LHC

Rene Poncelet and Andrei Popescu

Cavendish Laboratory, University of Cambridge,
J.J. Thomson Avenue, Cambridge CB3 0HE, United Kingdom

E-mail: poncelet@hep.phy.cam.ac.uk, popescu@hep.phy.cam.ac.uk

Abstract: Longitudinal polarisation of the weak bosons is a direct consequence of Electroweak symmetry breaking mechanism providing an insight into its nature, and is instrumental in searches for physics beyond the Standard Model. We perform a polarisation study of the diboson production in the pp $\to e^+\nu_e\mu^-\bar{\nu}_\mu$ process at NNLO QCD in the fiducial setup inspired by experimental measurements at ATLAS. This is the first polarisation study at NNLO. We employ the double-pole approximation framework for the polarised calculation, and investigate NNLO effects arising in differential distributions.

Keywords: QCD Phenomenology

ArXiv ePrint: 2102.13583

https://doi.org/10.1007/JHEP07(2021)023

Contents

JHEP07(2021)023

1 Introduction

Weak boson polarisation is under intense research both on the theoretical and experimental side. It is a handle to directly probe the Standard Model (SM) electroweak (EW) symmetry breaking mechanism and is instrumental in constraining the triple and quartic gauge boson couplings for beyond SM physics searches.

Several processes have been studied theoretically in the context of weak boson polarisation. Seminal papers covered the V+j process [1, 2]. Later on other processes were considered, such as diboson production [3–6], vector boson scattering (VBS) [7–9]. Top-quark decays are currently under investigation.

The amount of statistics of Run 2 at the LHC has enabled polarised measurement in relatively high cross section processes such as V+jet [10–13], boson [14, 15] and top-quark pair production [16, 17]. There are good prospects for polarised VBS signals at high-luminosity LHC [18] and there already are some results available [19]. It is impossible to directly select bosons with a specified polarisation, but methods like reweighting procedures [10–12, 20] and artificial intelligence techniques [21–24] allow for analysis of polarised signals. The main result is the extracted polarisation coefficients which are then compared to theoretical values. Close attention is paid to differential distributions for longitudinally polarised bosons, which is a direct probe of the EW symmetry breaking mechanism.

The production of weak boson pairs has been extensively studied in the literature. Next-to-leading order (NLO) [25–27], next-to-next-to-leading order (NNLO) [28–30] and

combined NLO EW and (N)NLO QCD [31, 32] computations are available for a variety of setups and observables. Resummation and parton shower effects have also been studied in the context of weak boson pair production [33–37]. Recent progress has been made in the computation of NLO corrections to cross sections for polarised bosons [5, 6]. There are two main obstacles that are in the way of direct theoretical calculations with polarised boson in the experimentally accessible signatures. Firstly, weak bosons are short-lived particles, and they can be observed only through their leptonic and hadronic decay signatures. They are produced off-shell and some adjustment is required to make sense of their polarisation state. Secondly, the signatures involve a non-resonant[1] background which cannot be removed in a simple manner, because it is essential for gauge invariance of the whole amplitude. Effects of the gauge invariance breakdown are severe [8]. The commonly used approach to tackle both issues is to use on-shell amplitudes which can be obtained either by restricting the integration phase space in the way of the narrow-width approximation [38, 39] or by means of an on-shell projection (OSP) [7, 8], also known as pole approximation. Regardless of the particular implementation, a method that uses on-shell amplitudes has an intrinsic uncertainty of $\mathcal{O}(\frac{\Gamma}{M})$ but it is still advantageous in comparison with the indirect approach involving reweighting which is used in experimental analysis as shown in the case of WZ production [8].

In this paper we address, for the first time, NNLO QCD correction for the polarised $\mathrm{W}^+\mathrm{W}^-$ production. We compute fiducial and differential cross sections at NNLO QCD accuracy for the LHC at 13 TeV and investigate what are the effects at this precision level. NNLO corrections are particularly important for the differential distributions in diboson production, where NLO scale uncertainty exceeds the intrinsic uncertainty related to the theoretical definition of boson polarisation. Additionally, we explore how narrow-width approximation performs in comparison with double-pole approximation which is assumed to be more accurate due to its incorporation of off-shell effects.

The structure of this paper is as follows. In section 2.1 we discuss approaches which we apply to define boson polarisations in the diboson production process. Then we specify our setup including the SM parameters, selection cuts, and a list of computational tools that we use. Section 3 is dedicated to our results. We present the integrated cross sections, and discuss the pure NNLO QCD corrections in section 3.2. We add the loop-induced channel and discuss its effects in section 3.3. In section 3.4 we compare the narrow-width approximation and the double-pole approximation for unpolarised weak bosons against an off-shell computation. In section 4 we summarise our findings.

2 Details of the calculation

2.1 Polarised weak bosons

In this paper we study the resonant production and subsequent decay of (un)polarised W^+W^--boson pairs at the LHC in the different flavour di-leptonic decay channel, i.e.

$$\mathrm{pp} \to \mathrm{W}^+\mathrm{W}^- + X \to \mathrm{e}^+\nu_\mathrm{e}\mu^-\bar{\nu}_\mu + X\,. \tag{2.1}$$

[1] Non-resonant as opposed to double-resonant. More precisely, single-resonant.

JHEP07(2021)023

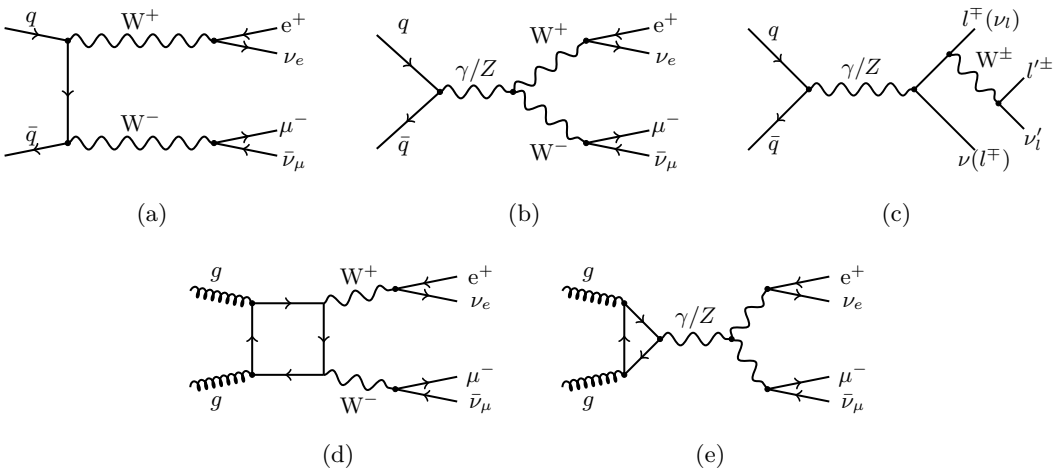

Figure 1. Selected diagrams contributing to the $pp \to e^+\nu_e\mu^-\bar{\nu}_\mu$ process. Diagrams (a,b) represent Born double-resonant contribution; (c) — general case of Born single-resonant contributions (background); (d,e) — loop-induced double-resonant contribution.

Figure 1(a) and figure 1(b) show the contributing *double-resonant* Feynman diagrams. The resonant process is a part of the more general off-shell production of the same leptonic final state

$$pp \to e^+\nu_e\mu^-\bar{\nu}_\mu + X\,. \tag{2.2}$$

This process has additional contributions from *single-resonant* diagrams, see figure 1(c). To define the production and decay of *polarised* intermediate vector-bosons in a gauge-invariant way both W-bosons are required to be on their mass-shell. We consider two commonly used approximations both resulting in on-shell amplitudes for polarised W-bosons: the so-called pole approximation or, in this case, *double-pole approximation* (DPA), and the *narrow-width approximation* (NWA). Both methods neglect *single-resonant* contributions present in the general process $pp \to e^+\nu_e\mu^-\bar{\nu}_\mu$ and introduce uncertainties which are formally of $\mathcal{O}(\Gamma_W/M_W)$. While this error estimate holds for inclusive observables, the uncertainty in differential distributions can be significantly larger.

NWA considers the limit $\Gamma_W/m_W \to 0$ in the cross section, thus neglecting $\mathcal{O}(\Gamma_W/m_W)$ terms, rendering the W-bosons on-shell, and factorizing the amplitudes and phase spaces of production and decay. The NWA works well with massive short-lived particles such as weak bosons and top-quarks, and so it is well suited for this study. By construction, this approximation performs poorly for observables which are sensitive to the off-shellness of the vector bosons. There exist extensions to the NWA, which attempt to include off-shell effects, such as the Madspin approach [40], which simulates the off-shell effects by using the Breit-Wigner sampling for the resonant propagator. We do not consider such an extension here. The production and decay are correlated through the boson's momenta and polarisations, schematically the amplitude factorizes as follows:

$$\mathcal{M}_{pp\to e^+\nu_e\mu^-\bar{\nu}_\mu} \sim \sum_{h,h'\in\Lambda} \mathcal{M}^{h,h'}_{pp\to W^+W^-}\Gamma^{h}_{W^+\to e^+\nu_e}\Gamma^{h'}_{W^-\to\mu^-\bar{\nu}_\mu}, \tag{2.3}$$

JHEP07(2021)023

where $h, h' \in \Lambda = \{+, -, L\}$ stand for the W-boson polarisations. By restricting the sum to specific choices for h, h' we define the polarised production and decay. We denote the coherent sum of the transverse polarisations $\{+, -\}$ as (T) and the longitudinal polarisation as (L).

The DPA [25, 41, 42] approach instead considers the off-shell phase space and introduces an approximation for the amplitudes alone. In order to guarantee gauge invariance, one defines an on-shell projection to map the off-shell kinematics of the decay products point-by-point to the on-shell kinematics. This allows the same factorization as in eq. (2.3) by neglecting *single-resonant* diagrams. Boson propagators with the off-shell kinematics are kept for modelling the Breit-Wigner shape of the off-shell amplitude.

DPA has an advantage over NWA in that it generates the off-shell kinematics, however it is not uniquely defined. The on-shell mapping has to be specified, whereas NWA approach is unambiguous. We will compare performance of these two methods in section 3.4.

For the polarisation study at NNLO we will use the DPA approach. We follow [7] in defining the on-shell projection, where the following conserved quantities are suggested:

1. the total diboson momentum $p_{\mathrm{W^+W^-}}$;

2. the direction of $p_{\mathrm{W^+}}$ momentum in diboson centre-of-mass frame (after a direct boost in Lab frame);

3. the angles of charged leptons w.r.t. to their parent boson momentum (in Lab frame) in their parent W-boson centre-of-mass frame (after a direct boost in Lab frame).

The algorithm goes as follows. Consider the diboson mass frame by a direct boost from Lab frame. In this frame individual boson momenta are equal and back-to-back, but generally not on-shell. To correct this, for each boson momenta, we fix the energy to be $\sqrt{s}/2$ and rescale the spatial part so that its length becomes $\frac{1}{2}\sqrt{s - 4M_{\mathrm{W}}^2}$, while the angles are kept untouched. These modifications do not affect the total momentum of the diboson system. Next, we turn to the decay products. In order to modify momenta of $\mathrm{e}^+, \nu_{\mathrm{e}}$ we reconstruct helicity frames in W^+-boson rest frame, and calculate angles of the positron using the original off-shell kinematics. While polar angle definition is unambiguous, the rotation of the XY-plane and thus the azimuthal angle is subject to specification. We discuss the azimuthal angle definition we use in appendix A. With the new on-shell W^+-boson momentum we construct the new positron momentum in the new parent boson rest frame with the original polar and azimuthal angles. The neutrino momentum is trivially inferred. Analogously, we build new momenta for the decay products of W^-.

The process under consideration allows for unambiguous on-shell mapping, but if there exists an ambiguity around combining the decay products into parent resonances, such as appearing in ZZ production or NLO EW radiation, the OSP should be revised. A treatment of non-factorisable corrections and a generic massive particle configuration can be found in [43].

The definition of the boson polarisation vectors entering the polarised production and decay amplitudes is not unambiguous and needs to be chosen. A particular choice, which

JHEP07(2021)023

we employ in this work, based on momenta in the laboratory frame, is

$$\begin{aligned}
\varepsilon_-^\mu &= \frac{1}{\sqrt{2}}\,(0, \cos\theta_V \cos\phi_V + \mathrm{i}\sin\phi_V, \cos\theta_V \sin\phi_V - \mathrm{i}\cos\phi_V, -\sin\theta_V)\ , \\
\varepsilon_+^\mu &= \frac{1}{\sqrt{2}}\,(0, -\cos\theta_V \cos\phi_V + \mathrm{i}\sin\phi_V, -\cos\theta_V \sin\phi_V - \mathrm{i}\cos\phi_V, \sin\theta_V)\ , \\
\varepsilon_{\mathrm{L}}^\mu &= \frac{1}{M}\,(p, E\sin\theta_V \cos\phi_V, E\sin\theta_V \sin\phi_V, E\cos\theta_V)\,,
\end{aligned} \tag{2.4}$$

for left, right, and longitudinal polarisations respectively. Here M, p, E are mass, total momentum, and energy of the weak boson, and θ_V, ϕ_V are its angles in a selected frame.

In this study we define polarisation vectors in the laboratory frame which is more accessible experimentally. However there exist other alternatives, e.g. the diboson centre-of-mass frame, which was also used in the experimental studies [19]. It has been observed that the frame choices tend to be rather complementary to each other in their discrimination power to isolate polarisations [6].

2.2 Numerical parameters

To fully specify our computational setup we give a summary of all numerical input parameters. We use the following set of particle parameters:

$$\begin{aligned}
M_{\mathrm{W}}^{\mathrm{os}} &= 80.3790\,\mathrm{GeV}, & \Gamma_{\mathrm{W}}^{\mathrm{os}} &= 2.0850\,\mathrm{GeV}, \\
M_{\mathrm{Z}}^{\mathrm{os}} &= 91.1876\,\mathrm{GeV}, & \Gamma_{\mathrm{Z}}^{\mathrm{os}} &= 2.4952\,\mathrm{GeV}, \\
M_{\mathrm{H}} &= 125\,\mathrm{GeV}, & \Gamma_{\mathrm{H}} &= 0.00407\,\mathrm{GeV}, \\
m_{\mathrm{t}} &= 173\,\mathrm{GeV}, & m_{\mathrm{b}} &= 4.7\,\mathrm{GeV};
\end{aligned} \tag{2.5}$$

where the boson parameters actually used in the calculation (pole values) are obtained by means of [44],

$$M_V = \frac{M_V^{\mathrm{OS}}}{\sqrt{1 + (\Gamma_V^{\mathrm{OS}}/M_V^{\mathrm{OS}})^2}}\,, \qquad \Gamma_V = \frac{\Gamma_V^{\mathrm{OS}}}{\sqrt{1 + (\Gamma_V^{\mathrm{OS}}/M_V^{\mathrm{OS}})^2}}; \tag{2.6}$$

for $V = \mathrm{W}, \mathrm{Z}$. All leptons are considered massless, which makes the results insensitive to the specific lepton flavours as long as they belong to different generations in order for the diboson reconstruction to remain unique. All other quarks $(\mathrm{u}, \mathrm{d}, \mathrm{c}, \mathrm{s})$ are considered massless.

We consider the 5-flavour PDF set `NNPDF31_[n]nlo_as_0118` (IDs: 303400, 303600) approximation for [N]NLO [45] as implemented in LHAPDF [46]. However, we use massive bottom quarks throughout the calculation to avoid contributions from off-shell top-quark pair production which would enter at NNLO and would be regarded as a separate process. Real emission contribution of massive $b\bar{b}$ quarks are neglected for the same reason. The numerical impact of the mismatch in the number of massless quarks between the PDF and the perturbative part is up to 0.6% at the total cross section level and up to 8% in the distribution tails (e.g. lepton p_T), however it is within by the factorisation scale uncertainty band, as we estimated at NLO. We would also like to point out that the scheme we use is —

JHEP07(2021)023

up to NLO — effectively the same as removing processes with a b-quark in the initial state, so with the chosen PDF set we are able to directly compare our results with [5] at NLO.

We use the complex mass scheme framework [47] and the couplings are fixed following the G_μ scheme with

$$G_\mu = 1.16638 \cdot 10^{-5}\,\mathrm{GeV}^{-2}. \tag{2.7}$$

Within the frameworks of NWA and DPA we set weak boson (W *and* Z) widths to zero in the calculation of couplings and the Weinberg angle, so they remain real.

Both factorisation and renormalisation scales are set to W pole mass: $\mu_F = \mu_R = M_\mathrm{W}$.

The cuts we use are presented as fiducial setup in ref. [5] inspired by ATLAS measurements [14]:

- minimum transverse momentum of the charged leptons, $p_{\mathrm{T},\ell} > 27\,\mathrm{GeV}$;
- maximum rapidity of the charged leptons, $|y_\ell| < 2.5$;
- minimum missing transverse momentum, $p_{\mathrm{T,miss}} > 20\,\mathrm{GeV}$;
- veto on events containing at least one jet candidate with $p_{\mathrm{T,j}} > 35\,\mathrm{GeV}, |\eta_\mathrm{j}| < 4.5$;
- minimum invariant mass of the charged lepton-pair system, $M_{\mathrm{e}^+\mu^-} > 55\,\mathrm{GeV}$.

Also, by construction, DPA and NWA contain an implicit cut on diboson invariant mass: $M_{\mathrm{W}^+\mathrm{W}^-} > 2 \cdot M_\mathrm{W}$.

The jet veto is used to reduce giant K-factors [30] otherwise mostly appearing at NLO but also driving up NNLO corrections. CKM matrix is assumed to be diagonal. Finally, the invariant mass cut reduces the Higgs background in the gg-initiated process. Note that we did not apply the $M_{\mathrm{W}^+\mathrm{W}^-} > 130\,\mathrm{GeV}$ cut for the gg-initiated process as suggested in [5] to exclude the Higgs peak region as it has little effect on the results.

2.3 Tools used in the calculation

The computation has been done using Stripper framework, a C++ implementation of the four-dimensional formulation of the sector-improved residue subtraction scheme [48, 49]. Stripper is a library which supplies a Monte-Carlo generator and automates the subtraction scheme, and it relies on external tools for calculating tree-level, one-loop and two-loop amplitudes. It has been successfully applied to the production of top-quark pairs [50, 51], inclusive jets [52], and three photons [53]. We use AvH library [54] to provide the Born amplitudes. The one-loop amplitudes are calculated using OpenLoops 2 [55–57], which we modified to extend its functionality to specify weak boson polarisations. The two-loop amplitudes for $q\bar{q}$-induced channel were provided by VVamp project [58].

Several checks have been performed both on the integrated cross section level and per phase space point. The total cross section for the off-shell setup calculated within Stripper framework was checked against Matrix at NNLO [59] in the inclusive setup. Our private build of OpenLoops 2 [55] was checked on the amplitude level against the private version of Recola used in [5] for various DPA setups. We checked our differential distributions at NLO against the ones provided in [5] as well as the total cross section results for various polarised setups.

JHEP07(2021)023

3 Results

In this section, we present phenomenological results for the polarised signals in W-pair production in the fiducial setup on the LHC at a hadronic centre of mass energy of 13 TeV.

Diboson production and its further decay into leptons is represented by the diagrams in figure 1. The loop-induced contribution in figures 1(d)–1(e) enters the calculation for the first time at NNLO in α_s. It is effectively a LO contribution which introduces substantial corrections. In what follows we will refer to NNLO corrections to diagrams in figures 1(a)–1(c) as to 'NNLO (without LI)', or just 'NNLO', and to corrections that include the loop-induced channel as to 'NNLO (with LI)' or 'NNLO+LI' corrections. The polarisation setups are identified by its polarised boson. We will abbreviate polarisation setups by two letters out of the set {U, T, L}, which correspond to unpolarised, transverse, and longitudinal boson polarisation respectively. For example, the singly-polarised setup with longitudinal W^+ boson will read 'LU'.

We provide LO, NLO, and NNLO results, the NNLO K-factor which is calculated as $\sigma_{\text{NNLO}}/\sigma_{\text{NLO}}$ at the central scale, and the NNLO+LI which includes the loop-induced channel. Scale uncertainties are calculated using the standard independent 7-point variation of μ_R, μ_F by a factor of 2 around the central scale, with the restriction $1/2 \leq \mu_R/\mu_F \leq 2$.

After discussing the fiducial cross section in the next section, we will turn our focus on 'NNLO (without LI)' corrections to differential distributions section 3.2. The effects of the loop-induced channel on differential distributions will be explored in section 3.3. Finally, a comparison on differential level of the DPA and NWA approaches against the off-shell computation will be performed in section 3.4.

3.1 Fiducial cross sections

The total cross-section results for various polarisation setups are presented in table 1. It also includes unpolarised calculations performed in the frameworks of DPA, NWA, and the off-shell calculation. Scale uncertainties are presented in percentage values with respect to the central scale result as sub- and superscripts. Monte-Carlo numerical errors on the central scale values are indicated in parentheses and correspond to the last significant digit of the result.

In the unpolarised setups we see that DPA undershoots the off-shell calculation by 2.5%. DPA is not supposed to fully match the off-shell calculation as it only includes double-resonant contributions relevant for the diboson production. This fraction persists after inclusion of NNLO corrections both with and without the loop-induced channel. In contrast to DPA, NWA result overshoots the off-shell result by 1%. In both cases the differences to the complete off-shell are well within their expectation of $\mathcal{O}(\Gamma_W/M_W)$, even though this estimate is only exact for inclusive phase space integration. The scale uncertainty decreases by a factor of 3 with NNLO corrections, however after introduction of the loop-induced channel bounces back to 80% and 50% of the NLO level for the higher and lower band correspondingly. The uncertainty band of the LI channel is almost identical across setups, but its relative contribution differs, affecting the overall theoretical uncertainty of the NNLO+LI result. Higher order corrections to the loop-induced channel, which are

JHEP07(2021)023

	NLO	NNLO	K_{NNLO}	LI	NNLO+LI
off-shell	$220.06(5)^{+1.8\%}_{-2.3\%}$	$225.4(4)^{+0.6\%}_{-0.6\%}$	1.024	$13.8(2)^{+25.5\%}_{-18.7\%}$	$239.1(4)^{+1.5\%}_{-1.2\%}$
unpol. (nwa)	$221.85(8)^{+1.8\%}_{-2.3\%}$	$227.3(6)^{+0.6\%}_{-0.6\%}$	1.025	$13.68(3)^{+25.5\%}_{-18.7\%}$	$241.0(6)^{+1.5\%}_{-1.1\%}$
unpol. (dpa)	$214.55(7)^{+1.8\%}_{-2.3\%}$	$219.4(4)^{+0.6\%}_{-0.6\%}$	1.023	$13.28(3)^{+25.5\%}_{-18.7\%}$	$232.7(4)^{+1.4\%}_{-1.1\%}$
W_L^+ (dpa)	$57.48(3)^{+1.9\%}_{-2.6\%}$	$59.3(2)^{+0.7\%}_{-0.7\%}$	1.032	$2.478(6)^{+25.5\%}_{-18.3\%}$	$61.8(2)^{+1.0\%}_{-0.8\%}$
W_L^- (dpa)	$63.69(5)^{+1.9\%}_{-2.6\%}$	$65.4(3)^{+0.8\%}_{-0.8\%}$	1.026	$2.488(6)^{+25.5\%}_{-18.3\%}$	$67.9(3)^{+0.9\%}_{-0.8\%}$
W_T^+ (dpa)	$152.58(9)^{+1.7\%}_{-2.1\%}$	$155.7(6)^{+0.7\%}_{-0.6\%}$	1.020	$11.19(2)^{+25.5\%}_{-18.8\%}$	$166.9(6)^{+1.6\%}_{-1.3\%}$
W_T^- (dpa)	$156.41(7)^{+1.7\%}_{-2.1\%}$	$159.7(6)^{+0.5\%}_{-0.6\%}$	1.021	$11.19(2)^{+25.5\%}_{-18.8\%}$	$170.9(6)^{+1.7\%}_{-1.3\%}$
$W_L^+W_L^-$ (dpa)	$9.064(6)^{+3.0\%}_{-3.0\%}$	$9.88(3)^{+1.3\%}_{-1.3\%}$	1.090	$0.695(2)^{+25.5\%}_{-18.8\%}$	$10.57(3)^{+2.9\%}_{-2.4\%}$
$W_L^+W_T^-$ (dpa)	$48.34(3)^{+1.9\%}_{-2.5\%}$	$49.4(2)^{+0.9\%}_{-0.7\%}$	1.021	$1.790(5)^{+25.5\%}_{-18.3\%}$	$51.2(2)^{+0.6\%}_{-0.8\%}$
$W_T^+W_L^-$ (dpa)	$54.11(5)^{+1.9\%}_{-2.5\%}$	$55.5(4)^{+0.6\%}_{-0.7\%}$	1.025	$1.774(5)^{+25.5\%}_{-18.3\%}$	$57.2(4)^{+0.7\%}_{-0.7\%}$
$W_T^+W_T^-$ (dpa)	$106.26(4)^{+1.6\%}_{-1.9\%}$	$108.3(3)^{+0.5\%}_{-0.5\%}$	1.019	$9.58(2)^{+25.5\%}_{-18.9\%}$	$117.9(3)^{+2.1\%}_{-1.6\%}$

Table 1. Total cross-sections (in fb) for the unpolarised, singly-polarised and doubly-polarised W^+W^- production at the LHC. Unpolarised calculation is performed in three ways: full off-shell, and using approximations: DPA, NWA. Polarised setups are calculated using DPA. Uncertainties are computed with 7-point scale variations by a factor of 2 around the central scale. K-factors are presented as ratios of NNLO QCD (without LI) over NLO integrated cross-sections. NNLO+LI represents the full $\mathcal{O}(\alpha_s^2)$ result.

formally of $\mathcal{O}(\alpha_s^3)$ (part of N^{3}LO), are expected to improve the uncertainty but are left for future work.

Next we consider singly-polarised setups. Missing interferences between longitudinal and transverse polarisations of $W^+(W^-)$ and restrictions on the leptonic phase space due to cuts, give rise to differences between the sum of the singly-polarised setups and the fully unpolarised DPA setup. The interference effects are of order 2% and are negative (positive) for singly-polarised $W^+(W^-)$. The NNLO K-factors are of the same magnitude across setups, with a slightly larger value for the longitudinal polarisations. The scale uncertainty features the same behaviour as for the unpolarised setups, except in the longitudinal setups it is not amplified by the loop-induced channel as it has a smaller relative contribution in comparison with transverse setups.

NNLO corrections (without LI) to the doubly-polarised setups can be estimated to be roughly 25% of NLO corrections, except for TL setup where NNLO corrections are a bit larger. It was shown that at NLO the doubly longitudinal polarisation of the diboson system is, among other polarisation setups, particularly affected by QCD corrections [5]. This is also true at NNLO as represented by the corresponding K-factor. As will be shown further, the profile of its corrections is also distinctly different on the differential level. The scale variation band goes down at NNLO, however the loop-induced channel brings it back to NLO level at both LL and TT setups, whereas for LT and TL setups it remains on the same level.

Of interest are the polarisation fractions, i.e. the fractions of the cross section for various polarised boson configurations. Although NNLO corrections differ among the different

JHEP07(2021)023

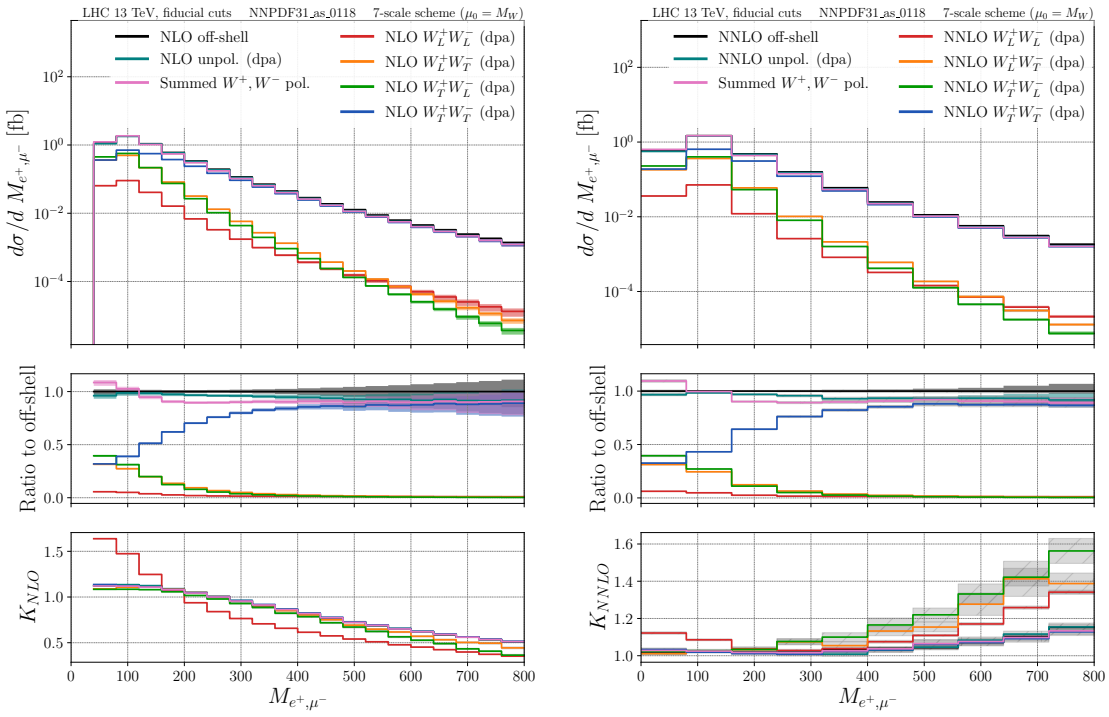

(a) at NLO (b) at NNLO (without LI)

Figure 2. Distribution of charged lepton pair invariant mass at different orders of QCD. Doubly-polarised setups are shown. From top-down: absolute value differential distribution, ratio to off-shell result, K-factor of the corresponding order. Monte-Carlo errors are shown in the middle and lower panes as grey bands. Scale variation bands are shown as coloured bands in the upper pane.

polarisations, there is no significant difference in the polarisation fractions with respect to NLO, indicating that the fractions are rather independent of higher order QCD corrections. In particular, the fraction of doubly-longitudinal polarised W, which gets the largest corrections, is still small.

3.2 NNLO QCD corrections to differential cross sections

In this section we will explore NNLO QCD effects on the differential distributions as they appear without the loop-induced channel. Observables which allow discrimination between different boson polarisations are of particular interest, theoretically and experimentally. The key quantity here is again the (differential) polarisation fractions. A general feature of differential polarisation fractions is that at high energies the longitudinal component vanishes as the weak bosons get effectively massless. Naturally, regions of large invariant mass or transverse momentum are populated by transversely polarised W-bosons. Close to the W-pair production threshold, where the diboson system is produced with small momentum, the contribution of the longitudinal component is largest.

This characteristic can be seen in the invariant mass distribution of the charged lepton pair, shown in figure 2. We show the NLO (left) and NNLO (right) predictions for the absolute cross section, the differential polarisation fraction, and the NLO and NNLO K-

JHEP07(2021)023

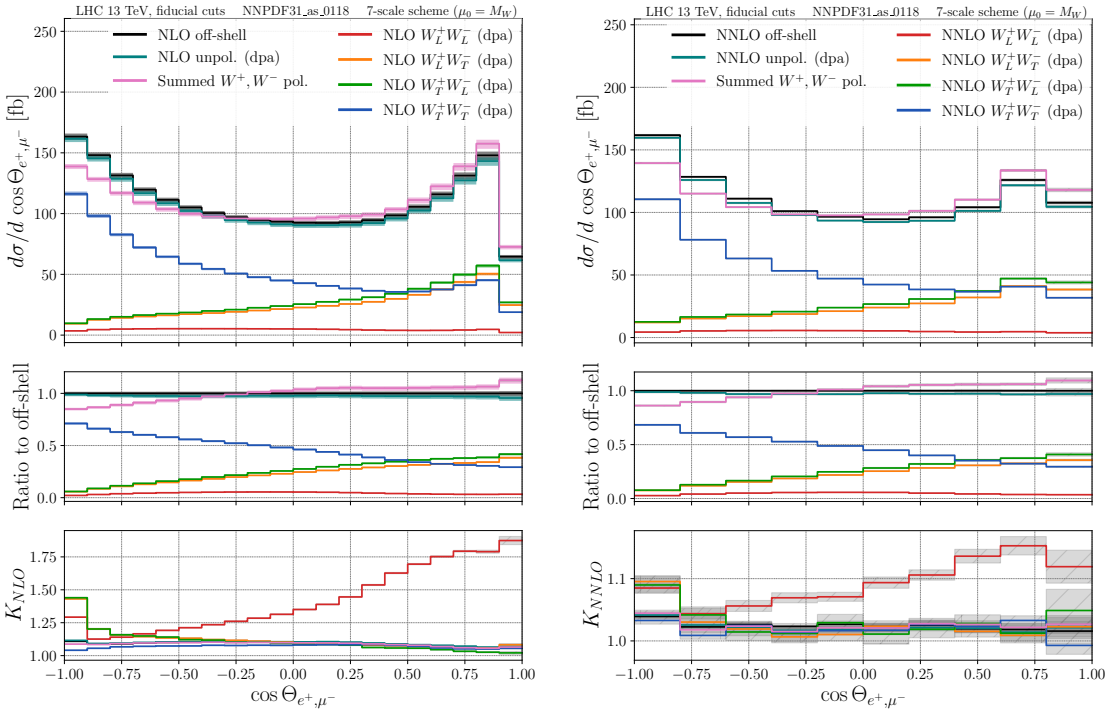

(a) at NLO (b) at NNLO (without LI)

Figure 3. Distribution of cosine of angle between charged leptons. Doubly-polarised setups are shown. Individual plot substructure is the same as in figure 2.

factors, respectively. At NNLO, the tail features strong positive corrections for the setups with longitudinally polarised bosons, reaching 50%. The scale variation bands get notably reduced across polarisation setups, particularly in the tail of the distribution, however there the off-shell calculation still shows a substantial scale uncertainty. The shape of the NNLO K-factor in the tail is mainly driven by the fixed scale choice which is not optimal for this phase space region. Finally, the doubly-longitudinal setup shows a larger correction in the low invariant mass region, which was also the case at NLO.

It is worth pointing out that this is the region where the most of the production cross section is coming from. This implies that observables which are sensitive to the threshold region, or bulk region, are especially well suited to study boson polarisations. In particular, this includes angular observables of the final state charged leptons which both have a strong sensitivity to polarisations and are shaped by the bulk region.

For example, consider the angular separation between two charged leptons in figure 3. Back-to-back configurations, i.e. where $\cos\Theta_{e^+,\mu^-} \approx -1$, are dominated by the doubly-transverse setup, while the regions where the two leptons are aligned, have large contributions from setups containing a longitudinal boson. NNLO corrections reduce the scale dependence to the sub-percent level and show a rather small and flat K-factor. A notable exception is the LL setup as it receives strong corrections up to 10–15% in magnitude and shape. However, due to its overall small contribution it does not affect the polarisation fractions.

JHEP07(2021)023

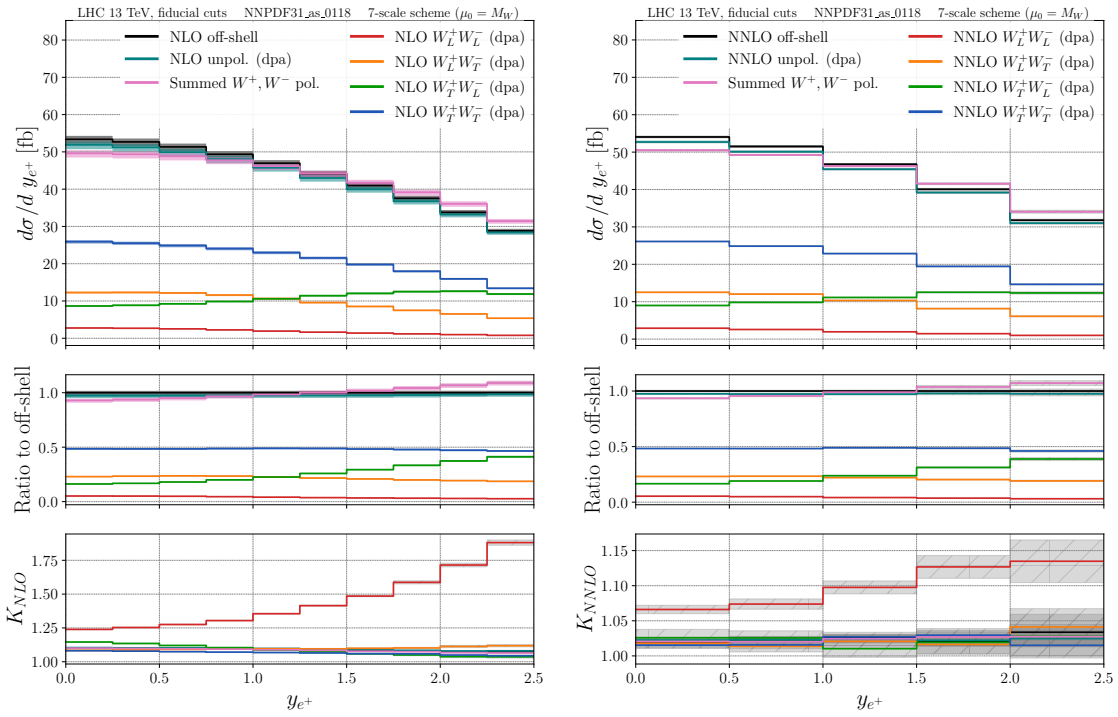

(a) at NLO (b) at NNLO (without LI)

Figure 4. Symmetrised distribution of e^+ rapidity at different orders of QCD. Doubly-polarised setups are shown. Individual plot substructure is the same as in figure 2.

Similar effects can be observed in the rapidity distributions. Figure 4 features the symmetrised version of e^+ rapidity distribution. Here, LL polarisation receives a significant correction for higher rapidities.

To point out another feature of the longitudinally polarised signals, it is instructive to investigate transverse momentum distributions for leptons and W-bosons. First, consider the transverse momentum distributions of the charged leptons $p_T(e^+)$ and $p_T(\mu^-)$. In figure 5 we show $p_T(e^+)$ (left) and the ratio of the differential cross sections (right)

$$\frac{d\sigma_{p_T(\mu^-)}}{d\sigma_{p_T(e^+)}} \equiv \frac{d\sigma/dp_T(\mu^-)}{d\sigma/dp_T(e^+)} \,. \tag{3.1}$$

There is a striking difference in the ratio for the LT polarised setup, which can be explained through asymmetries in the decay of W^+ and W^-. The charged leptons have a larger probability to get emitted forward (in the flight direction of the parent W boson) for transversely polarised bosons than for longitudinal ones. This can be seen in figure 5(c) and figure 5(d) demonstrating the distribution in the opening angle between the charged leptons and their parent W-boson (for precise definition of the angles, see appendix A). Thus we expect the transverse boson to produce a harder p_T spectrum for its decay products than the longitudinal one, i.e. the ratio $d\sigma_{p_T(\mu^-)}/d\sigma_{p_T(e^+)}$ is expected to be smaller than 1 for TL setup and larger than 1 for LT setup. This effect is magnified by the asymmetry

JHEP07(2021)023

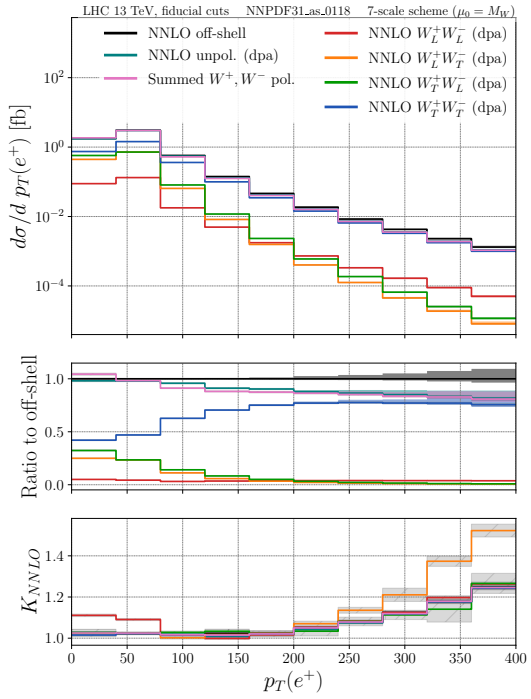

(a) Positron transverse momentum

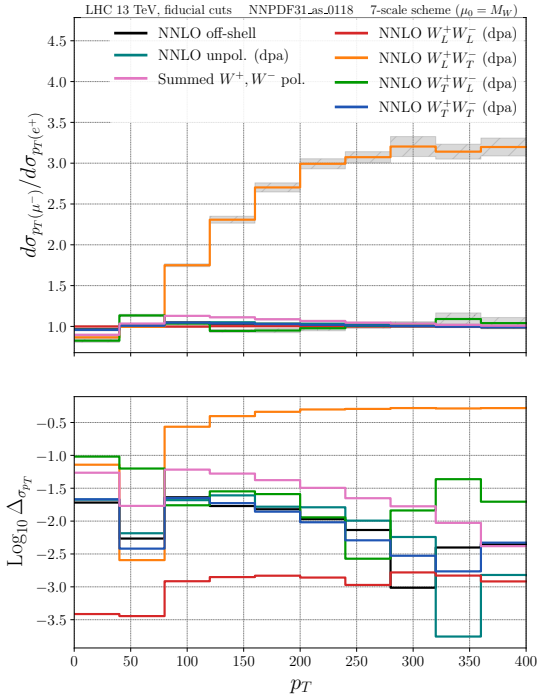

(b) Ratio of the muon and positron transverse momentum distributions

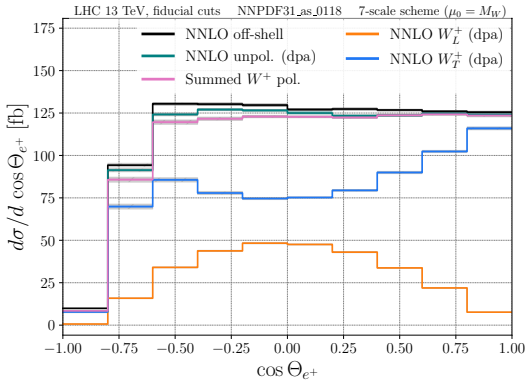

(c) $\cos\angle(\mathrm{e}^+, \mathrm{W}^+)$

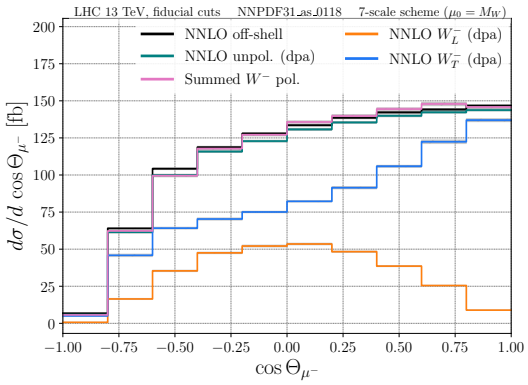

(d) $\cos\angle(\mu^-, \mathrm{W}^-)$

Figure 5. (Upper row) Distribution of lepton transverse momentum at NNLO (without LI) for e^+ (left) and its comparison with distribution for μ^- (right). Individual plot substructure in (a) is the same as in figure 2. The plot (b) structure is the following: the upper plot features the ratio of muon over positron transverse momenta distributions; the lower plot in (b) features $\mathrm{Log}_{10}\left|\frac{\sigma_{p_T}(\mathrm{e}^+)-\sigma_{p_T}(\mu^-)}{\sigma_{p_T}(\mathrm{e}^+)+\sigma_{p_T}(\mu^-)}\right|$, where σ_{p_T} is the differential transverse momentum distribution. Doubly-polarised setups are shown. (Lower row) Distributions of charged lepton scattering angle cosine calculated in the parent W-boson CM frame at NNLO (without LI) for e^+ (left) and μ^- (right). Parent boson singly-polarised setups are shown. Individual plots show the absolute value distributions.

JHEP07(2021)023

between angle of emission distribution in W^+ and W^- transverse setups and is caused by the universally left-handed nature of W-bosons produced at the LHC [1]. Unfortunately, as in the case of the invariant mass distribution, the longitudinal contributions vanish at high transverse momentum, which makes it more difficult to exploit this observation in experimental measurements.

3.3 Effects of the loop-induced contribution

The loop-induced gg-channel only appears at α_s^2 order and has quite a substantial effect on the cross-section. Its effects on various differential distributions have been already investigated in [5]. In this section we will briefly comment on it again in the context of the NNLO calculation.

Usually, the loop-induced channel provides a glimpse into the NNLO effects in general. However, due to the simple kinematics structure of the diboson production, especially its double-resonant contribution, the Born kinematics configuration is not enough to get the right distribution shape for many observables. Using table 1 it can be pointed out that loop-induced channel increases scale variation bands up to almost NLO QCD level in all setups except the ones that contain exactly one longitudinally polarised weak boson.

In figure 6 we present relative corrections to the differential distribution of positron transverse momentum, with respect to the NLO calculation. Here we observe that NNLO calculation has brought the scale variation down, and that it is within a reasonable distance from NLO given the scale uncertainty. However, the loop-induced contribution drastically changes the picture, and its effect depends on the polarisation setup.

Setups that include a longitudinal W-boson receive mild corrections from the loop-induced channel at low p_T but are hugely affected in the tail ($p_T > 120\,\text{GeV}$). Also, the scale variation band in the tail becomes larger than for any other approximation. As is illustrated by figure 7, this is caused mainly by the top-quark loop contribution, which becomes relevant at $p_T(l^\pm) \sim 100\,\text{GeV}$. It does not affect the results or the scale uncertainty at the total cross section level ant it is not visible in any of the distribution representing the bulk of the cross section.

Setups containing a transverse W-boson represent a different correction in the loop-induced channel at NNLO. Here we observe an overall positive shift of order 10% which diminishes by the end of the distribution. This behaviour is expectedly replicated by the unpolarised setup as the transverse contribution dominates the cross section.

Similar effects can be observed in the charged leptons invariant mass distribution.

Next, we show the rapidity of e^+ distribution in figure 8. The setups containing transverse polarisations as well as the unpolarised setup feature about a 10% positive correction which is compatible with what we observed at the bulk of the positron p_T distribution. The case is different however for setups containing a longitudinal W. In particular, the LL polarisation receives a strong correction, which is expected due to its overall large K-factor in table 1. The gg loop-induced channel follows the shape of NNLO corrections except in the TT setup, where the loop induced corrections appear to be larger than NLO.

JHEP07(2021)023

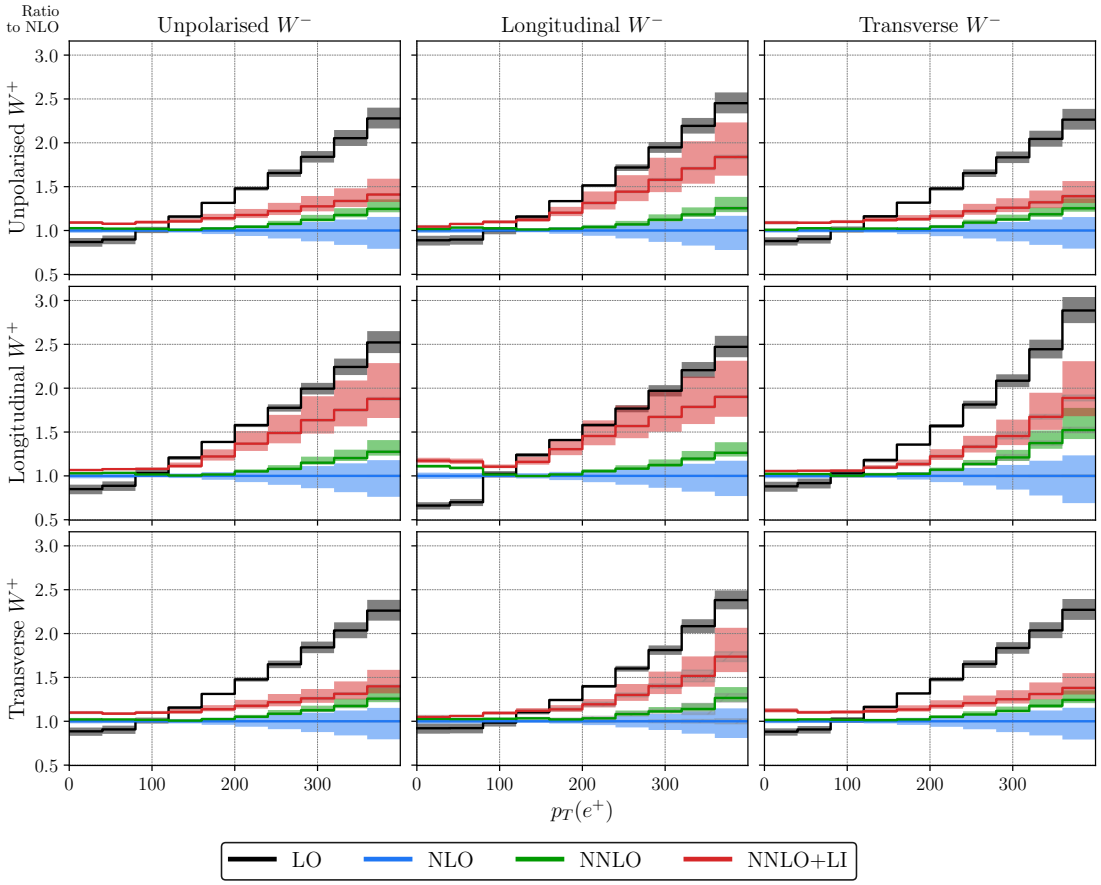

Figure 6. Ratio to NLO of e^+ transverse momentum distribution at various orders of perturbative QCD. Each of 9 panes represents a selected polarisation setup calculated within DPA framework. W^+ and W^- polarisation setups $\{U, L, T\}$ are cycled across vertical and horizontal plots respectively. Coloured regions represent scale variation bands, and grey bands — Monte-Carlo uncertainties.

Finally, in angular distributions related to the lepton emission angles we see an overall shift which does not affect the distribution shapes. However, a notable difference can be observed in azimuthal separation between the charged leptons which is a distribution highly susceptible to interference effects even at the inclusive level. In figure 9 we note that LI channel has a large overall shift in TT and unpolarised setups and features a rather interesting behaviour in LL setup. LI channel barely has any effect on LL setup at $\phi_{e^+,\mu^-} < 1$ but then introduces sizeable corrections up to 15%. We will encounter a similar shape in the discussion about DPA and NWA at unpolarised level in section 3.4.

Overall, we see a need for higher corrections of order α_s^3 in the gg loop-induced channel, to bring the scale variation down. This is left for future work.

3.4 Comparison between DPA and NWA

As we discussed in section 2.1, double-pole and narrow-width approximations consider the same set of double-resonant diagrams, however they are different in how they generate the

JHEP07(2021)023

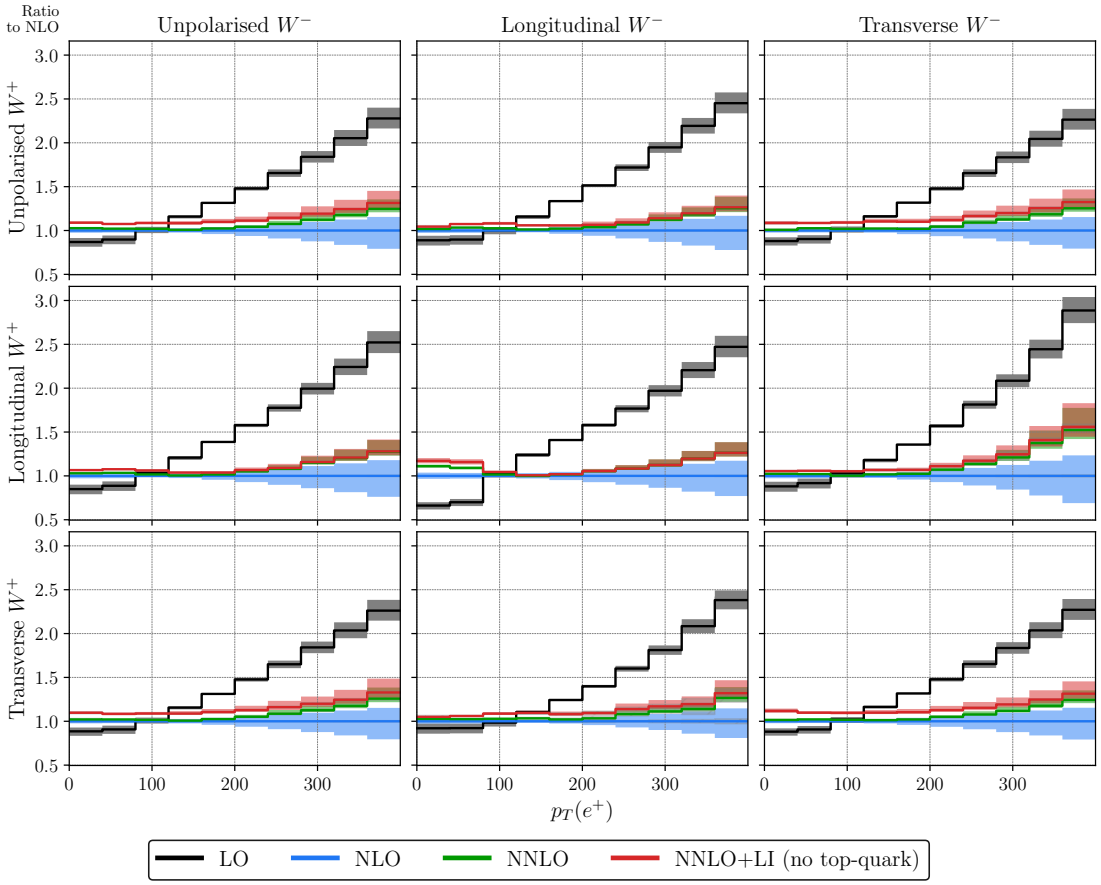

Figure 7. Ratio to NLO of e^+ transverse momentum distribution at various orders of perturbative QCD with top-quark loop contribution removed. Same plot structure as in figure 6.

phase space. DPA is able to incorporate off-shell effects via generating off-shell kinematics and subsequently projecting it on-shell to ensure gauge invariance of the amplitude. NWA is thus considered to be a less precise approach [5]. It is therefore instructive to compare NWA and DPA in the diboson production setting to inspect differences in their performance.

The approximations differ on the integrated level which we discussed in section 3.1. Moving on to the differential distributions, we note that by construction, NWA approach, is unable to describe the weak boson invariant masses, so we will not discuss this observable. In fact, due to the absence of single-resonant diagrams, DPA also does not describe the full off-shell amplitude, and produces a rather symmetrical shape that is different from the off-shell result [5].

There are distributions where NWA and DPA show the same shape but feature an overall shift that we see on the integrated level. The symmetrised rapidity and azimuthal angle of emission are such examples and are shown at NLO for positron in figure 10. The reader can also find a discussion on the definition of azimuthal angle of emission in appendix A.

For these distributions, it makes sense to compare them normalised by their integrated values. The bottom panes of figure 10 show that the normalised shapes between DPA and

JHEP07(2021)023

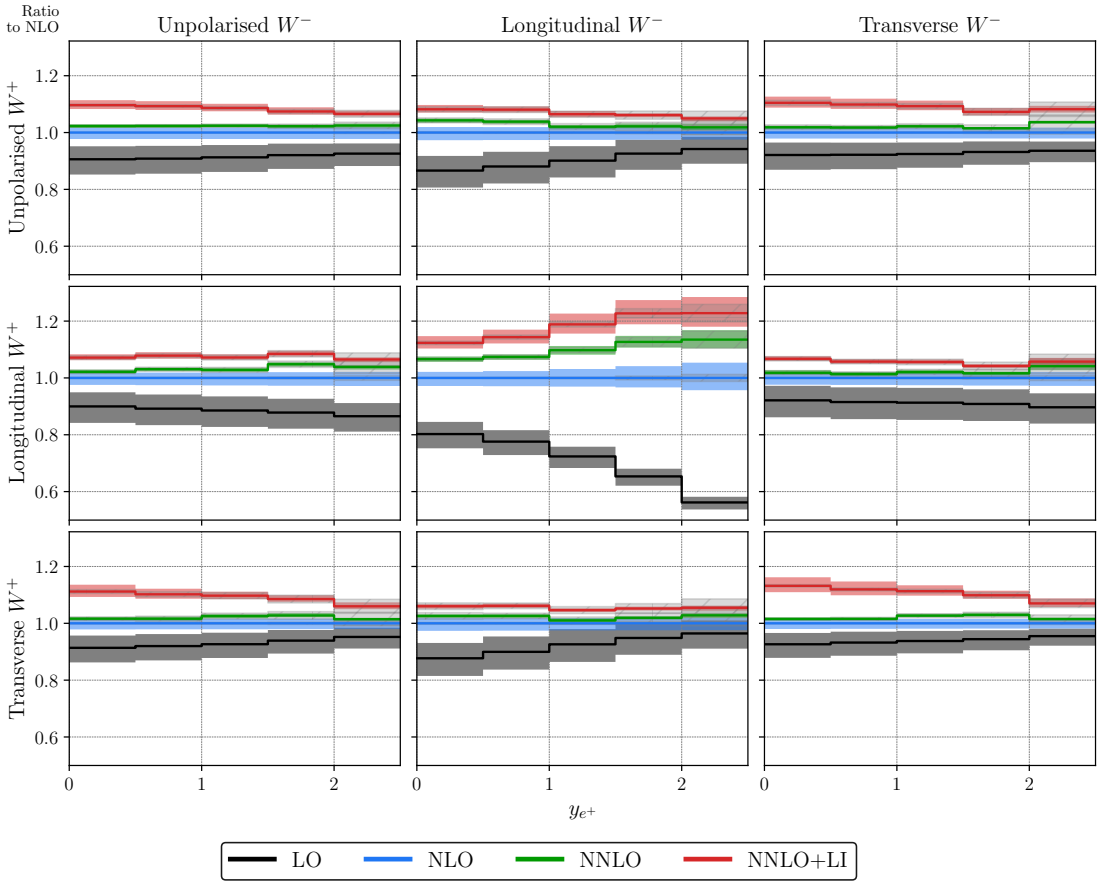

Figure 8. Ratio to NLO of symmetrised e^+ rapidity distribution at various orders of perturbative QCD. Same plot structure as in figure 6.

NWA agree well within their Monte-Carlo errors at NLO. This behaviour is replicated at NNLO also with the inclusion of the loop-induced channel.

Another distribution that showcases similarities in DPA and NWA performance is the cosine of angle between the charged leptons featured on figure 11(b). Here the approximations agree with each other across the entire range except for the first and the last bins as one can see from the "normalised to off-shell" plot. Fiducial cuts affect the last bin and are responsible for its large MC errors, but in the case of the first one there is a true difference. This is independent of QCD order and can be observed already at LO. Perhaps, the DPA mapping underperformes in the point where leptons are emitted in the opposite directions.

In figure 11(a) we show a comparison between the charged lepton emission angle in the DPA and NWA frameworks. DPA features a distribution that is slightly further from the off-shell result. Near the first bin the distribution is affected by the fiducial cuts and so the approximations become further away from the off-shell calculation. The same conclusions can be reached for angular distributions of the muon and are replicated at NNLO QCD including the loop-induced channel.

JHEP07(2021)023

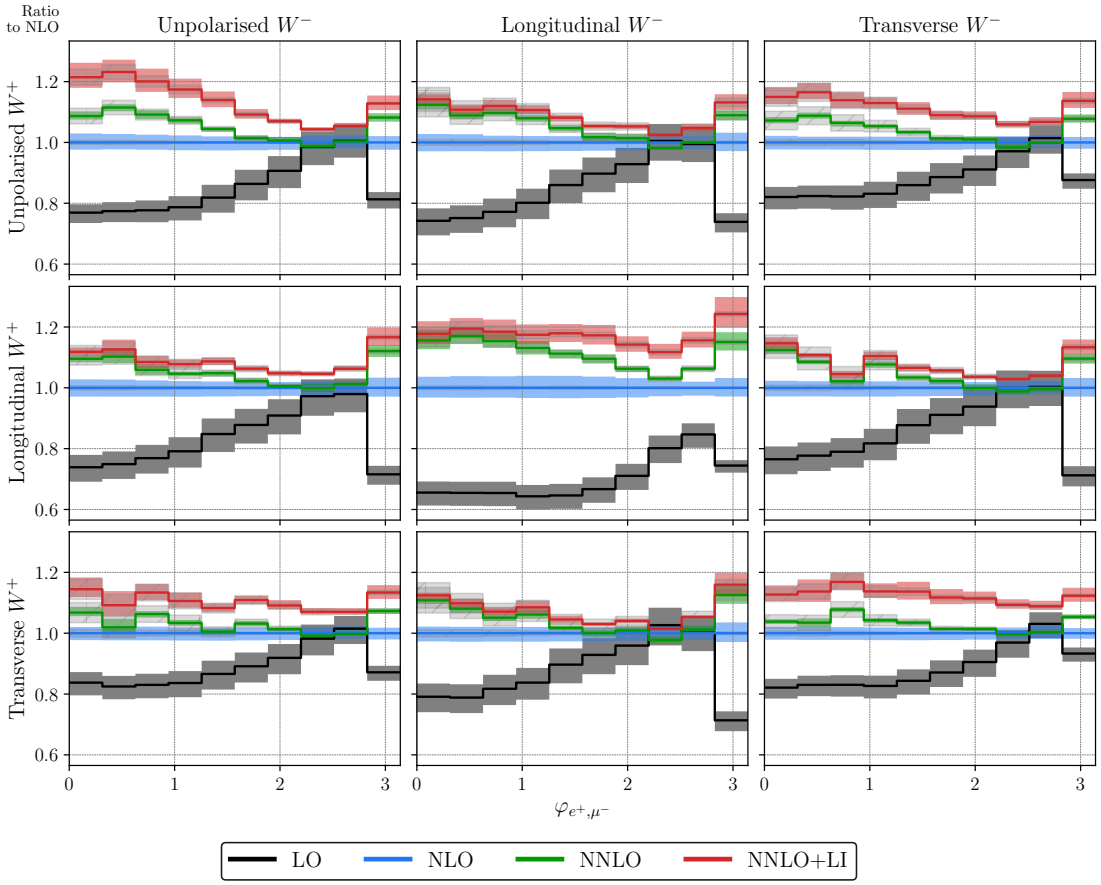

Figure 9. Ratio to NLO of azimuthal separation between charged leptons at various orders of perturbative QCD. Same plot structure as in figure 6.

A notable deviation can be observed between the setups at the beginning of various transverse momentum and invariant mass distributions, which represent the bulk of the cross section. In figure 12(b) we present the leading lepton p_T which shows that at $p_T < 50\,\text{GeV}$ NWA overshoots the off-shell calculation, whereas DPA undershoots. This region is the origin of the total cross section results, as at higher p_T the distribution falls nearly exponentially. DPA and NWA differ by 2% in the tail of the distribution and both deviate significantly from the full off-shell calculation due to single-resonant effects [26]. Similar effects of the two approximations can be observed in the diboson invariant mass distribution. W-boson transverse momentum distribution features the same interplay between DPA and NWA, however here the approximations are closer to the off-shell result. NNLO K-factor shapes are the same across three setups, however the loop-induced channel appears to make a difference in the distribution tail where DPA and NWA receive 20% larger corrections. This effect also observed in the W-boson transverse momentum profile.

Finally, quite an interesting difference in the behaviour between DPA and NWA can be observed in the azimuthal angular separation between charged leptons. In figure 12(a) one can see that the ratio to full off-shell calculation is distinctly different between NWA

JHEP07(2021)023

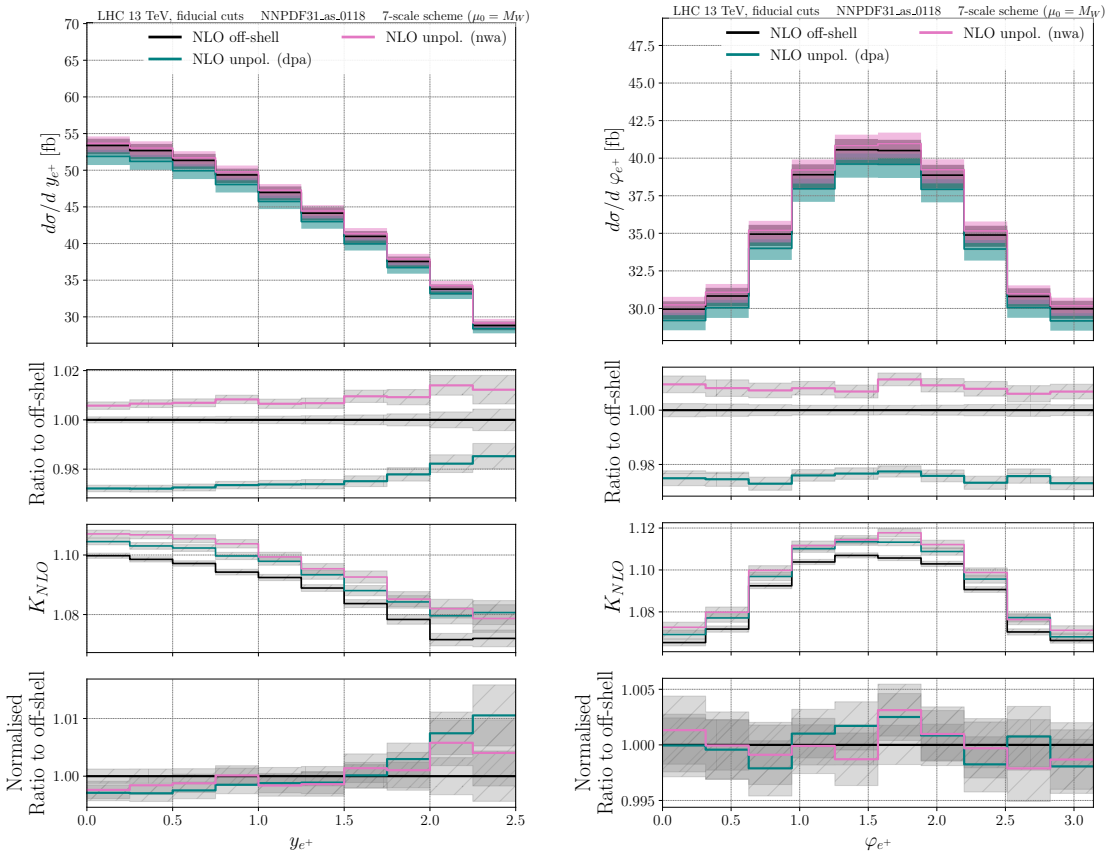

(a) Symmetrised rapidity of positron (NLO)

(b) Symmetrised azimuthal angle of positron emission in its parent boson CM (NLO)

Figure 10. Comparison between off-shell calculation, DPA, and NWA for selected distributions. Top three panes have the same structure as in figure 2; the bottom plot shows the ratio distributions to off-shell calculation normalised according to integrated cross-section value.

and DPA for $\phi_{e^+,\mu^-} > 0.75$. They have matching values up until this threshold and diverge until the end of the distribution at $\phi = \pi$. In this region of disagreement, NWA overshoots the off-shell computation. Expectedly, it appears to be the peak of the distribution, thus contributing to the overall large NWA integrated cross section value. This behaviour persists with introduction of higher orders. K-factor both for NNLO corrections and for the inclusion of loop-induced contribution has the same shape across setups and thus does not introduce any differences to the shapes of the ratio plots.

4 Conclusion

In this paper we compute, for the first time, polarised diboson production through NNLO in QCD within the framework of double-pole approximation. In the calculations we considered a fiducial phase space that emulates experimental setting which was already used in recent theoretical and experimental studies of the polarised processes.

JHEP07(2021)023

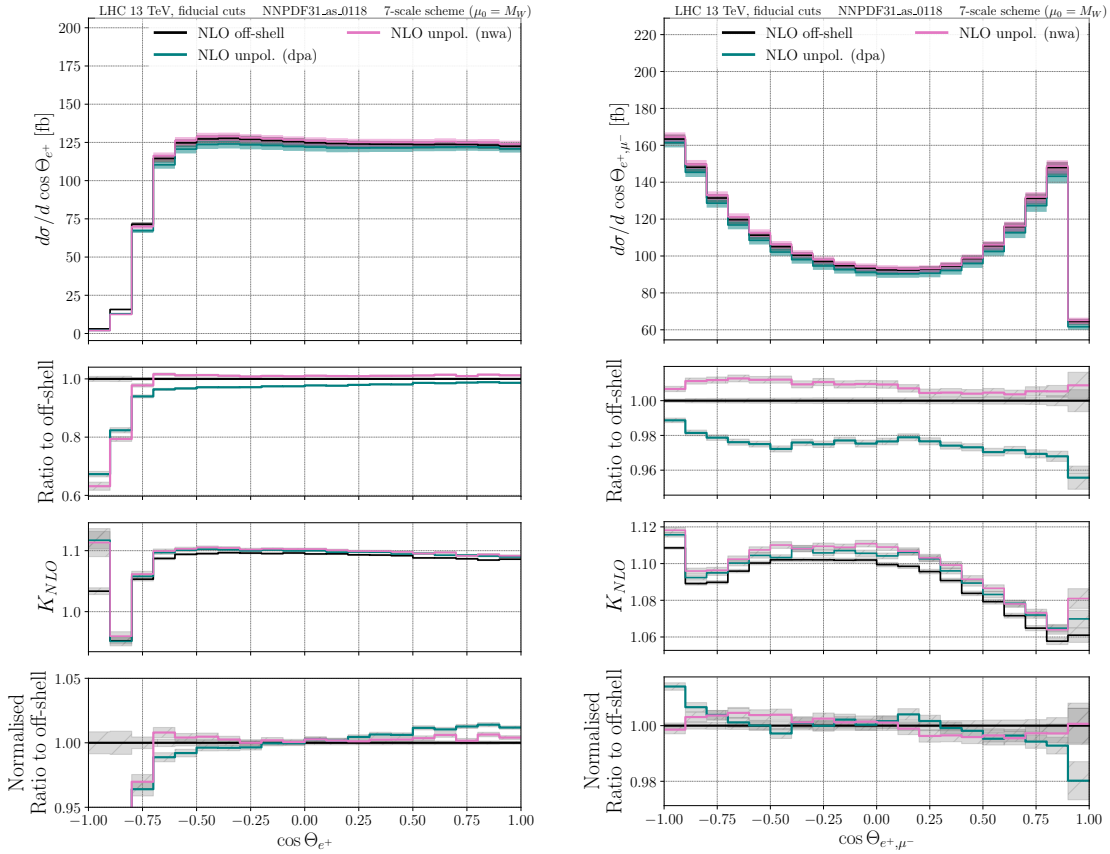

(a) Cosine of positron emission polar angle (b) Cosine of angle between charged leptons (NLO)

Figure 11. Comparison between off-shell calculation, DPA, and NWA for selected distributions. Same plot substructure as in figure 10.

NNLO corrections effects are twofold. With the exclusion of the loop-induced channel, the corrections show a controlled and predictable behaviour, particularly in the regions that represent the bulk of the cross section. Among notable effects we would point out significant corrections to the tail of transverse momentum and invariant mass distributions, especially in the case of longitudinal setups. The scale uncertainty is brought down by a factor of 3 across all polarisation setups.

However, the loop-induced channel changes the picture at NNLO significantly. Being technically a leading order contribution, it massively increases the scale uncertainty of both integrated and differential results. This behaviour prompts for introduction of $\mathcal{O}(\alpha_s^3)$ corrections (NLO) to the loop-induced channel, which is left for future work.

Finally, we compared the narrow-width and double-pole approximations in the unpolarised setup. NWA overshoots the off-shell result by 1%, while DPA is lower by 2.5%, which falls within their expected approximation error. Distributions look similar in the case of rapidity and charged lepton emission angles. We observed a significant deviation between approaches at low transverse momenta and pointed out a local difference between

JHEP07(2021)023

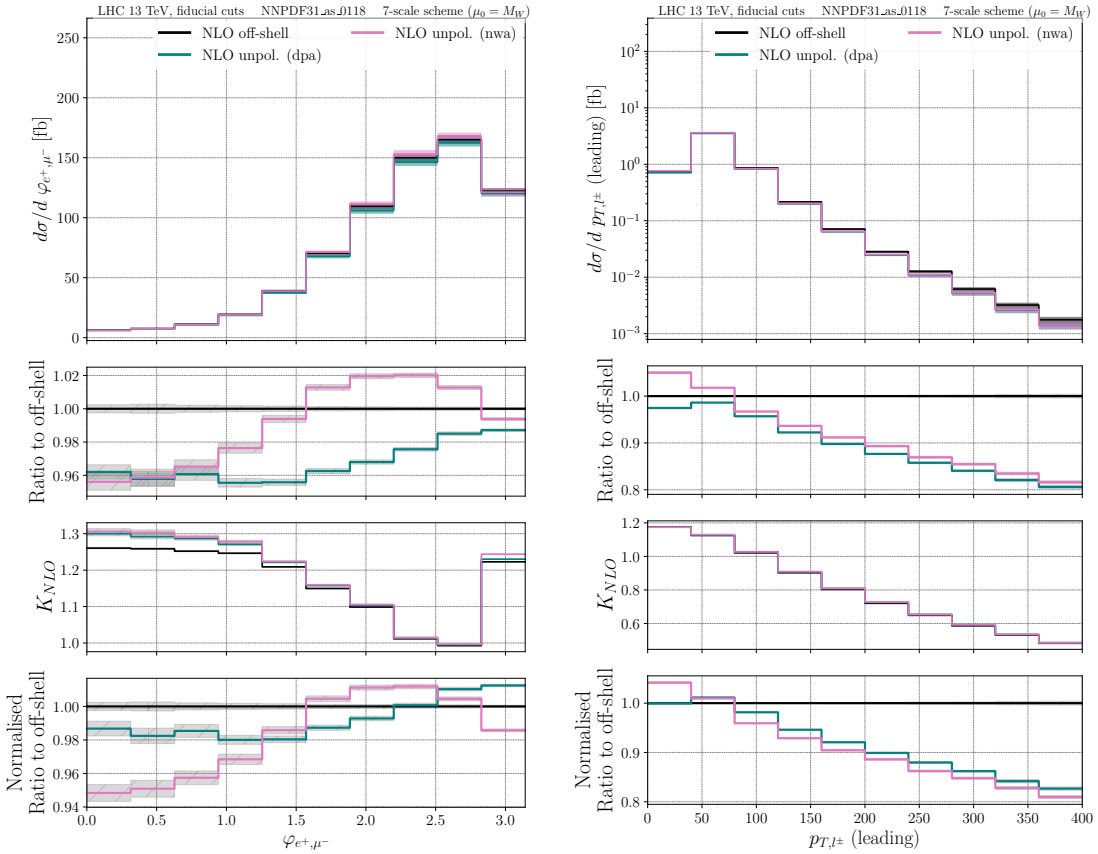

(a) Azimuthal separation between charged leptons (NLO)

(b) Leading lepton transverse momentum (NLO)

Figure 12. Comparison between off-shell calculation, DPA, and NWA for selected distributions. Same plot substructure as in figure 10.

the charged lepton azimuthal separation, where NWA features a more volatile behaviour in comparison with DPA, undershooting and overshooting the off-shell result. Generally, we observe similar results between the methods with only slight variation in particular observables and generally the same behaviour with respect to their ability to describe the full off-shell result.

Acknowledgments

We are grateful to Jean-Nicolas Lang, Giovanni Pelliccioli, and Ansgar Denner for providing their polarisation-capable private version of RECOLA and giving us explanations. We would like to thank Jonas Lindert for technical support with OPENLOOPS. We acknowledge helpful discussions with Alexander Mitov and useful comments from Heribertus Bayu Hartanto and the Cambridge Pheno Group. This research has received funding from the European Research Council (ERC) under the European Union's Horizon 2020 Research and Innovation Programme (grant agreement no. 683211). A.P. is also supported by the Cambridge Trust, and Trinity College Cambridge.

JHEP07(2021)023

A Azimuthal angle of emission

In this appendix we briefly discuss ways to define charged lepton emission angles.

There are two reference frames commonly used in the literature: the helicity (HE) frame and Collins-Soper (CS) frame. The helicity coordinate system is defined in [1]. As we observed in the literature, it is common, however, to simplify its construction by using a fixed reference momentum. In order to be able to compare the distributions, we follow suit. Here is the full algorithm we use to construct the $X'Y'Z'$ helicity frame.

Denote the first proton momentum as reference, and define Z' axis by the direction of W-boson in the Lab frame. Then proton momenta P_1, P_2 are boosted into the W-boson rest frame where they become P_1', P_2'. We build $\vec{Y}'$ axis in the direction of $[\vec{P}_1' \times \vec{P}_2']$ vector which is a perpendicular to the plane based on boosted proton momenta. Finally, X' axis is defined such that $X'Y'Z'$ coordinate system is right-handed, i.e. $\vec{X}' \sim [\vec{Y}' \times \vec{Z}']$.

Another choice is the Collins-Soper frame which originates from [60]. In short, the construction goes by boosting proton momenta into the boson rest frame where they are denoted by P_1', P_2'. Then Z' axis is defined as a bisection between vectors $\{\vec{P}_1', -\vec{P}_2'\}$. The X' axis is chosen as a bisection between $\{-\vec{P}_1', -\vec{P}_2'\}$. Finally Y' axis is uniquely defined to complete the right-handed system.

We find useful the discussion of these frames in [3], where the authors also present the distributions corresponding to different frame choices.

References

[1] Z. Bern et al., *Left-Handed W Bosons at the LHC*, *Phys. Rev. D* **84** (2011) 034008 [arXiv:1103.5445] [INSPIRE].

[2] W.J. Stirling and E. Vryonidou, *Electroweak gauge boson polarisation at the LHC*, *JHEP* **07** (2012) 124 [arXiv:1204.6427] [INSPIRE].

[3] J. Baglio and N. Le Duc, *Fiducial polarization observables in hadronic WZ production: A next-to-leading order QCD+EW study*, *JHEP* **04** (2019) 065 [arXiv:1810.11034] [INSPIRE].

[4] J. Baglio and L.D. Ninh, *Polarization observables in WZ production at the* 13 *TeV LHC: Inclusive case*, *Commun. in Phys.* **30** (2020) 35 [arXiv:1910.13746] [INSPIRE].

[5] A. Denner and G. Pelliccioli, *Polarized electroweak bosons in W^+W^- production at the LHC including NLO QCD effects*, *JHEP* **09** (2020) 164 [arXiv:2006.14867] [INSPIRE].

[6] A. Denner and G. Pelliccioli, *NLO QCD predictions for doubly-polarized WZ production at the LHC*, *Phys. Lett. B* **814** (2021) 136107 [arXiv:2010.07149] [INSPIRE].

[7] A. Ballestrero, E. Maina and G. Pelliccioli, *W boson polarization in vector boson scattering at the LHC*, *JHEP* **03** (2018) 170 [arXiv:1710.09339] [INSPIRE].

[8] A. Ballestrero, E. Maina and G. Pelliccioli, *Polarized vector boson scattering in the fully leptonic WZ and ZZ channels at the LHC*, *JHEP* **09** (2019) 087 [arXiv:1907.04722] [INSPIRE].

JHEP07(2021)023

[9] S. De, V. Rentala and W. Shepherd, *Measuring the polarization of boosted, hadronic W bosons with jet substructure observables*, arXiv:2008.04318 [INSPIRE].

[10] CMS collaboration, *Measurement of the Polarization of W Bosons with Large Transverse Momenta in W+Jets Events at the LHC*, *Phys. Rev. Lett.* **107** (2011) 021802 [arXiv:1104.3829] [INSPIRE].

[11] ATLAS collaboration, *Measurement of the polarisation of W bosons produced with large transverse momentum in pp collisions at $\sqrt{s} = 7$ TeV with the ATLAS experiment*, *Eur. Phys. J. C* **72** (2012) 2001 [arXiv:1203.2165] [INSPIRE].

[12] CMS collaboration, *Angular coefficients of Z bosons produced in pp collisions at $\sqrt{s} = 8$ TeV and decaying to $\mu^+\mu^-$ as a function of transverse momentum and rapidity*, *Phys. Lett. B* **750** (2015) 154 [arXiv:1504.03512] [INSPIRE].

[13] ATLAS collaboration, *Measurement of the angular coefficients in Z-boson events using electron and muon pairs from data taken at $\sqrt{s} = 8$ TeV with the ATLAS detector*, *JHEP* **08** (2016) 159 [arXiv:1606.00689] [INSPIRE].

[14] ATLAS collaboration, *Measurement of fiducial and differential W^+W^- production cross-sections at $\sqrt{s} = 13$ TeV with the ATLAS detector*, *Eur. Phys. J. C* **79** (2019) 884 [arXiv:1905.04242] [INSPIRE].

[15] ATLAS collaboration, *Measurement of $W^\pm Z$ production cross sections and gauge boson polarisation in pp collisions at $\sqrt{s} = 13$ TeV with the ATLAS detector*, *Eur. Phys. J. C* **79** (2019) 535 [arXiv:1902.05759] [INSPIRE].

[16] ATLAS collaboration, *Measurement of the W boson polarisation in $t\bar{t}$ events from pp collisions at $\sqrt{s} = 8$ TeV in the lepton + jets channel with ATLAS*, *Eur. Phys. J. C* **77** (2017) 264 [*Erratum ibid.* **79** (2019) 19] [arXiv:1612.02577] [INSPIRE].

[17] CMS collaboration, *Measurement of the W boson helicity fractions in the decays of top quark pairs to lepton + jets final states produced in pp collisions at $\sqrt{s} = 8$TeV*, *Phys. Lett. B* **762** (2016) 512 [arXiv:1605.09047] [INSPIRE].

[18] P. Azzi et al., *Report from Working Group 1: Standard Model Physics at the HL-LHC and HE-LHC*, *CERN Yellow Rep. Monogr.* **7** (2019) 1 [arXiv:1902.04070] [INSPIRE].

[19] CMS collaboration, *Measurements of production cross sections of polarized same-sign W boson pairs in association with two jets in proton-proton collisions at $\sqrt{s} = 13$ TeV*, *Phys. Lett. B* **812** (2021) 136018 [arXiv:2009.09429] [INSPIRE].

[20] ATLAS collaboration, *Measurement of Top Quark Polarization in Top-Antitop Events from Proton-Proton Collisions at $\sqrt{s} = 7$ TeV Using the ATLAS Detector*, *Phys. Rev. Lett.* **111** (2013) 232002 [arXiv:1307.6511] [INSPIRE].

[21] J. Searcy, L. Huang, M.-A. Pleier and J. Zhu, *Determination of the WW polarization fractions in $pp \to W^\pm W^\pm jj$ using a deep machine learning technique*, *Phys. Rev. D* **93** (2016) 094033 [arXiv:1510.01691] [INSPIRE].

[22] J. Lee et al., *Polarization fraction measurement in same-sign WW scattering using deep learning*, *Phys. Rev. D* **99** (2019) 033004 [arXiv:1812.07591] [INSPIRE].

[23] J. Lee et al., *Polarization fraction measurement in ZZ scattering using deep learning*, *Phys. Rev. D* **100** (2019) 116010 [arXiv:1908.05196] [INSPIRE].

[24] M. Grossi, J. Novak, B. Kersevan and D. Rebuzzi, *Comparing traditional and deep-learning techniques of kinematic reconstruction for polarization discrimination in vector boson scattering*, *Eur. Phys. J. C* **80** (2020) 1144 [arXiv:2008.05316] [INSPIRE].

JHEP07(2021)023

[25] M. Billóni, S. Dittmaier, B. Jäger and C. Speckner, *Next-to-leading order electroweak corrections to $pp \to W^+W^- \to 4$ leptons at the LHC in double-pole approximation*, *JHEP* **12** (2013) 043 [arXiv:1310.1564] [INSPIRE].

[26] B. Biedermann et al., *Next-to-leading-order electroweak corrections to $pp \to W^+W^- \to 4$ leptons at the LHC*, *JHEP* **06** (2016) 065 [arXiv:1605.03419] [INSPIRE].

[27] A. Bierweiler, T. Kasprzik, J.H. Kühn and S. Uccirati, *Electroweak corrections to W-boson pair production at the LHC*, *JHEP* **11** (2012) 093 [arXiv:1208.3147] [INSPIRE].

[28] F. Caola, K. Melnikov, R. Röntsch and L. Tancredi, *QCD corrections to W^+W^- production through gluon fusion*, *Phys. Lett. B* **754** (2016) 275 [arXiv:1511.08617] [INSPIRE].

[29] M. Grazzini, S. Kallweit, S. Pozzorini, D. Rathlev and M. Wiesemann, *W^+W^- production at the LHC: fiducial cross sections and distributions in NNLO QCD*, *JHEP* **08** (2016) 140 [arXiv:1605.02716] [INSPIRE].

[30] M. Grazzini, S. Kallweit, J.M. Lindert, S. Pozzorini and M. Wiesemann, *NNLO QCD + NLO EW with Matrix+OpenLoops: precise predictions for vector-boson pair production*, *JHEP* **02** (2020) 087 [arXiv:1912.00068] [INSPIRE].

[31] A. Denner, S. Dittmaier, P. Maierhöfer, M. Pellen and C. Schwan, *QCD and electroweak corrections to WZ scattering at the LHC*, *JHEP* **06** (2019) 067 [arXiv:1904.00882] [INSPIRE].

[32] A. Denner, R. Franken, M. Pellen and T. Schmidt, *NLO QCD and EW corrections to vector-boson scattering into ZZ at the LHC*, *JHEP* **11** (2020) 110 [arXiv:2009.00411] [INSPIRE].

[33] E. Re, M. Wiesemann and G. Zanderighi, *NNLOPS accurate predictions for W^+W^- production*, *JHEP* **12** (2018) 121 [arXiv:1805.09857] [INSPIRE].

[34] S. Kallweit, E. Re, L. Rottoli and M. Wiesemann, *Accurate single- and double-differential resummation of colour-singlet processes with MATRIX+RADISH: W^+W^- production at the LHC*, *JHEP* **12** (2020) 147 [arXiv:2004.07720] [INSPIRE].

[35] S. Bräuer, A. Denner, M. Pellen, M. Schönherr and S. Schumann, *Fixed-order and merged parton-shower predictions for WW and WWj production at the LHC including NLO QCD and EW corrections*, *JHEP* **10** (2020) 159 [arXiv:2005.12128] [INSPIRE].

[36] M. Chiesa, C. Oleari and E. Re, *NLO QCD+NLO EW corrections to diboson production matched to parton shower*, *Eur. Phys. J. C* **80** (2020) 849 [arXiv:2005.12146] [INSPIRE].

[37] J.H. Kühn, F. Metzler, A.A. Penin and S. Uccirati, *Next-to-Next-to-Leading Electroweak Logarithms for W-Pair Production at LHC*, *JHEP* **06** (2011) 143 [arXiv:1101.2563] [INSPIRE].

[38] A. Denner, S. Dittmaier, M. Roth and D. Wackeroth, *Predictions for all processes $e^+e^- \to 4$ fermions $+\gamma$*, *Nucl. Phys. B* **560** (1999) 33 [hep-ph/9904472] [INSPIRE].

[39] A. Denner, S. Dittmaier, M. Roth and L.H. Wieders, *Electroweak corrections to charged-current $e^+e^- \to 4$ fermion processes: Technical details and further results*, *Nucl. Phys. B* **724** (2005) 247 [*Erratum ibid.* **854** (2012) 504] [hep-ph/0505042] [INSPIRE].

[40] D. Buarque Franzosi, O. Mattelaer, R. Ruiz and S. Shil, *Automated predictions from polarized matrix elements*, *JHEP* **04** (2020) 082 [arXiv:1912.01725] [INSPIRE].

[41] W. Beenakker, F.A. Berends and A.P. Chapovsky, *Radiative corrections to pair production of unstable particles: results for $e^+e^- \to 4$ fermions*, *Nucl. Phys. B* **548** (1999) 3 [hep-ph/9811481] [INSPIRE].

JHEP07(2021)023

[42] A. Denner and S. Dittmaier, *Electroweak Radiative Corrections for Collider Physics*, *Phys. Rept.* **864** (2020) 1 [arXiv:1912.06823] [INSPIRE].

[43] S. Dittmaier and C. Schwan, *Non-factorizable photonic corrections to resonant production and decay of many unstable particles*, *Eur. Phys. J. C* **76** (2016) 144 [arXiv:1511.01698] [INSPIRE].

[44] D.Y. Bardin, A. Leike, T. Riemann and M. Sachwitz, *Energy Dependent Width Effects in e^+e^- Annihilation Near the Z Boson Pole*, *Phys. Lett. B* **206** (1988) 539 [INSPIRE].

[45] Particle Data Group collaboration, *Review of Particle Physics*, *Phys. Rev. D* **98** (2018) 030001 [INSPIRE].

[46] A. Buckley et al., *LHAPDF6: parton density access in the LHC precision era*, *Eur. Phys. J. C* **75** (2015) 132 [arXiv:1412.7420] [INSPIRE].

[47] A. Denner and S. Dittmaier, *The Complex-mass scheme for perturbative calculations with unstable particles*, *Nucl. Phys. B Proc. Suppl.* **160** (2006) 22 [hep-ph/0605312] [INSPIRE].

[48] M. Czakon, *A novel subtraction scheme for double-real radiation at NNLO*, *Phys. Lett. B* **693** (2010) 259 [arXiv:1005.0274] [INSPIRE].

[49] M. Czakon and D. Heymes, *Four-dimensional formulation of the sector-improved residue subtraction scheme*, *Nucl. Phys. B* **890** (2014) 152 [arXiv:1408.2500] [INSPIRE].

[50] A. Behring, M. Czakon, A. Mitov, A.S. Papanastasiou and R. Poncelet, *Higher order corrections to spin correlations in top quark pair production at the LHC*, *Phys. Rev. Lett.* **123** (2019) 082001 [arXiv:1901.05407] [INSPIRE].

[51] M. Czakon, A. Mitov and R. Poncelet, *NNLO QCD corrections to leptonic observables in top-quark pair production and decay*, *JHEP* **05** (2021) 212 [arXiv:2008.11133] [INSPIRE].

[52] M. Czakon, A. van Hameren, A. Mitov and R. Poncelet, *Single-jet inclusive rates with exact color at $\mathcal{O}(\alpha_s^4)$*, *JHEP* **10** (2019) 262 [arXiv:1907.12911] [INSPIRE].

[53] H.A. Chawdhry, M.L. Czakon, A. Mitov and R. Poncelet, *NNLO QCD corrections to three-photon production at the LHC*, *JHEP* **02** (2020) 057 [arXiv:1911.00479] [INSPIRE].

[54] M. Bury and A. van Hameren, *Numerical evaluation of multi-gluon amplitudes for High Energy Factorization*, *Comput. Phys. Commun.* **196** (2015) 592 [arXiv:1503.08612] [INSPIRE].

[55] F. Buccioni et al., *OpenLoops 2*, *Eur. Phys. J. C* **79** (2019) 866 [arXiv:1907.13071] [INSPIRE].

[56] F. Cascioli, P. Maierhofer and S. Pozzorini, *Scattering Amplitudes with Open Loops*, *Phys. Rev. Lett.* **108** (2012) 111601 [arXiv:1111.5206] [INSPIRE].

[57] F. Buccioni, S. Pozzorini and M. Zoller, *On-the-fly reduction of open loops*, *Eur. Phys. J. C* **78** (2018) 70 [arXiv:1710.11452] [INSPIRE].

[58] T. Gehrmann, A. von Manteuffel and L. Tancredi, *The two-loop helicity amplitudes for $q\bar{q}' \to V_1V_2 \to 4$ leptons*, *JHEP* **09** (2015) 128 [arXiv:1503.04812] [INSPIRE].

[59] T. Gehrmann et al., *W^+W^- Production at Hadron Colliders in Next to Next to Leading Order QCD*, *Phys. Rev. Lett.* **113** (2014) 212001 [arXiv:1408.5243] [INSPIRE].

[60] J.C. Collins and D.E. Soper, *Angular Distribution of Dileptons in High-Energy Hadron Collisions*, *Phys. Rev. D* **16** (1977) 2219 [INSPIRE].

JHEP07(2021)023